Supplementary online material

Deterministic switching in bismuth ferrite nanoislands

Alessio Morelli [†,*], *Florian Johann* [‡,§], *Stuart R. Burns* [†,‖], *Alan Douglas* [†], *J. Marty Gregg* [†]

[†] Centre for Nanostructured Media, School of Mathematics and Physics, Queen's University Belfast, University Road, Belfast BT7 1NN, United Kingdom

[‡] Max Planck Institute of Microstructure Physics, D-06120 Halle, Germany

§ Asylum Research, an Oxford Instruments company, Borsigstrasse 15a, 65205 Wiesbaden, Germany

‖ School of Materials Science and Engineering, University of New South Wales, Sydney NSW 2052, Australia

Piezo-hysteresis loop on film and island

Acquired at 1V AC amplitude at 22kHz.

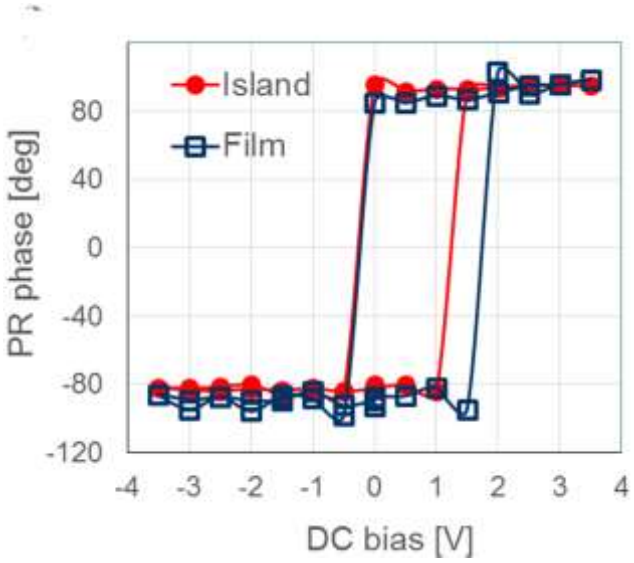

Figure S1. Piezo-hysteresis loop acquired on film (square open symbols) and on island (round closed symbols) with 1V AC amplitude at 22kHz.

Extended dataset of the anti-vortex results in Figure 4

Data in Figure 4b,c,d,e have been extracted by 2um x 2um PFM images, acquired at a scan speed of 0.5Hz, with 1V AC amplitude at 22kHz.

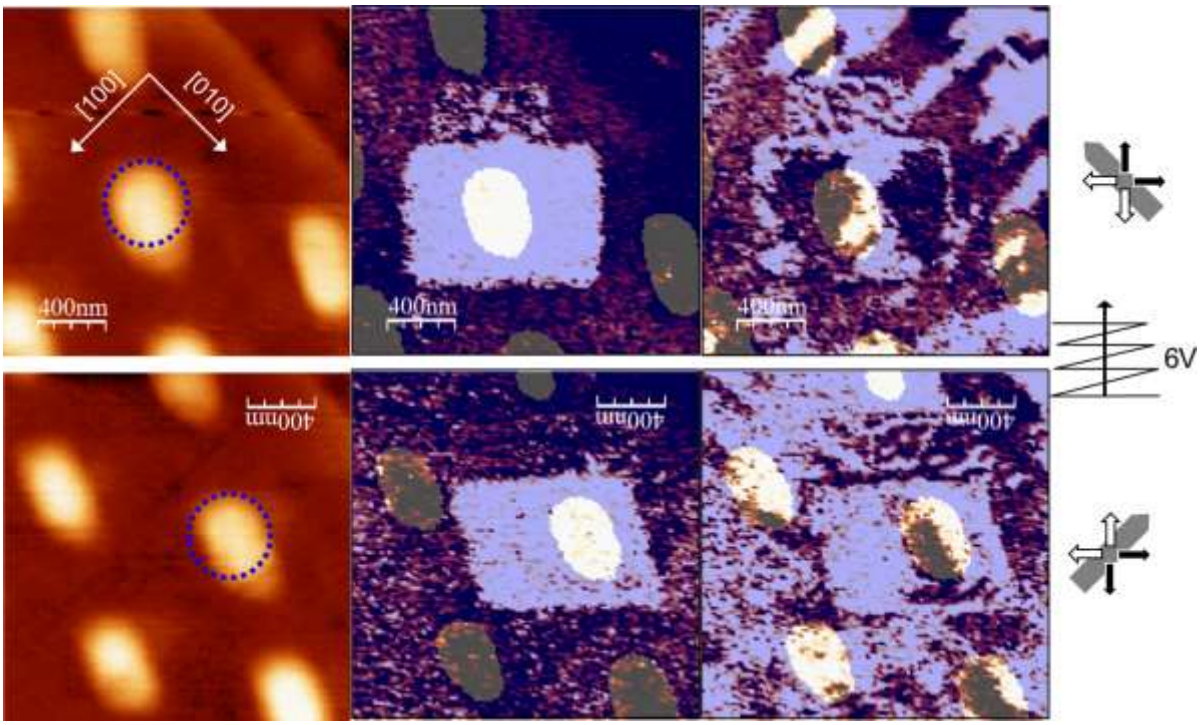

Figure S2. Topography, Vertical PFM phase, Lateral PFM phase (left to right) with probe along [0 $\bar{1}$ 0] (top) and [$\bar{1}$ 00] (bottom) after poling at +6V, with slow raster axis along [$\bar{1}$ $\bar{1}$ 0].

Poling with [100] and [010] slow raster axis

Poling with slow raster axis along [100] or [010] leads to multidomain configuration similarly to the stripe-like configuration as resulting from switching experiments on film surface in BFO films with all polarization variants allowed. In fact in this case the trailing field favors more than one variant. In Figure S2, results of such experiments on islands (400nm diameter, 30nm height) obtained with same fabrication procedure from a 100nm BFO/SRO/$DyScO_3$ film.

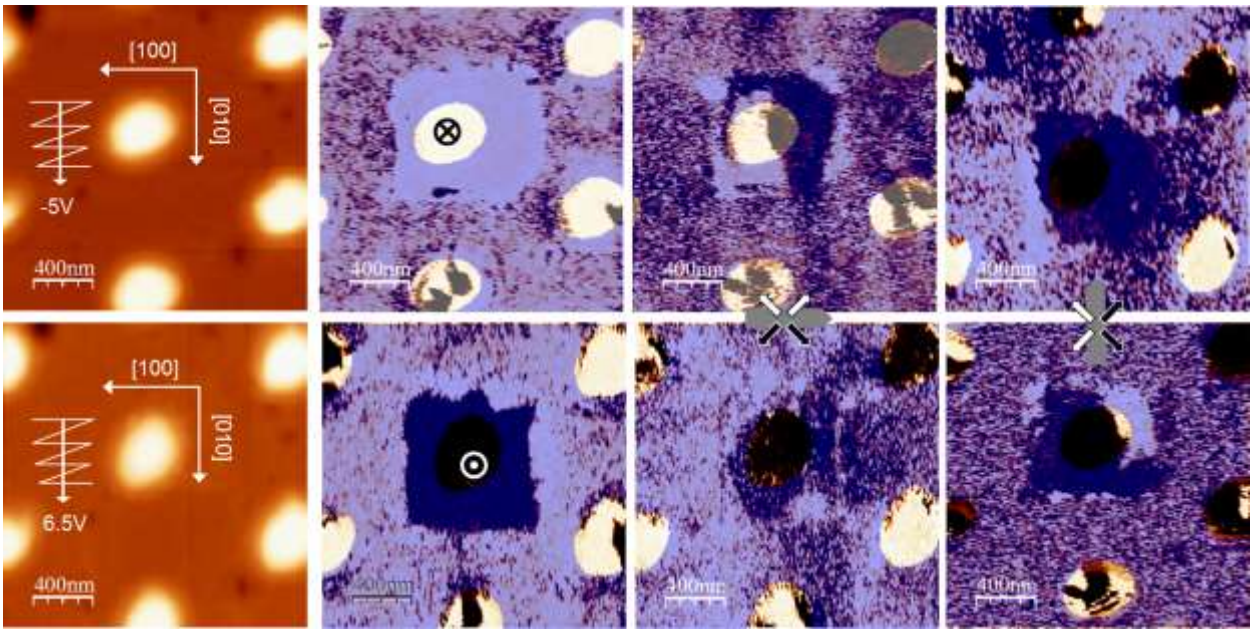

Figure S3. Topography, Vertical PFM phase, Lateral PFM phase with probe along [0 $\bar{1}$ 0] and [$\bar{1}$ 00] (left to right) after poling at -5V (top) and +6.5V (bottom), with slow raster axis along [010].

Extended dataset of the variant selection results in Figure 5

Data in Figure 5b,c,d,e have been extracted by 2um x 2um PFM images, acquired at a scan speed of 0.5Hz, with 1V AC amplitude at 22kHz.

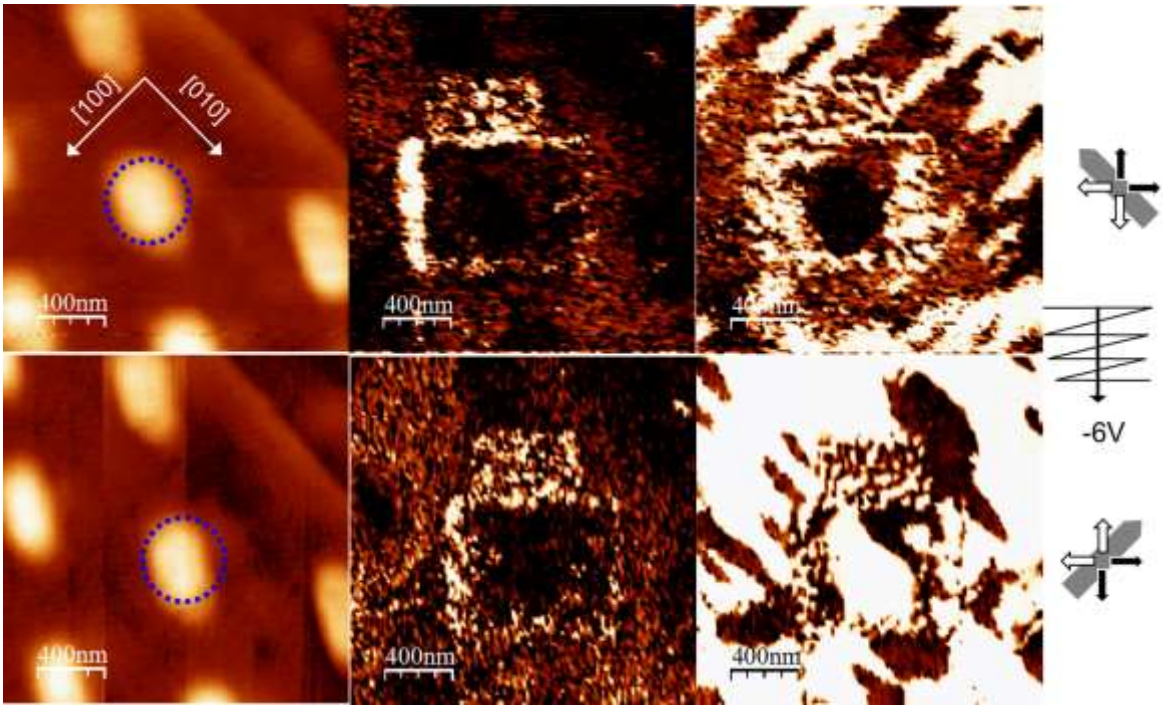

Figure S4. Topography, Vertical PFM phase, Lateral PFM phase (left to right) with probe along [0 $\overline{1}$ 0] (top) and [$\overline{1}$ 00] (bottom) after poling at -6V, with slow raster axis along [110].

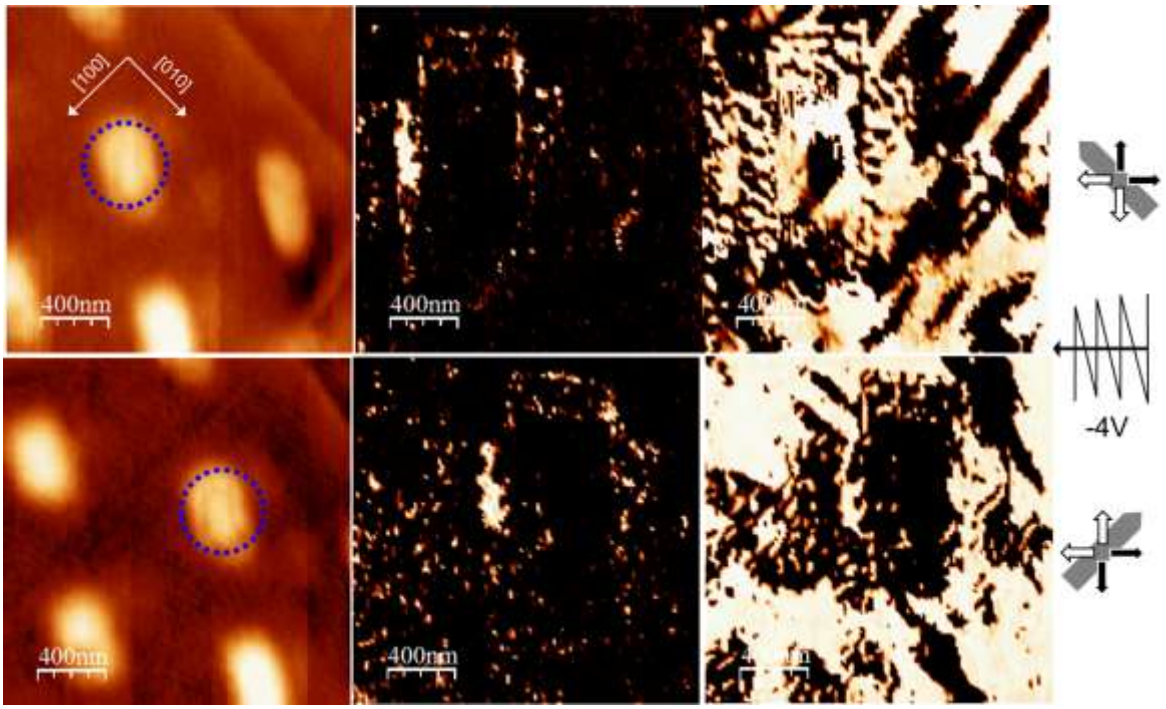

Figure S5. Topography, Vertical PFM phase, Lateral PFM phase (left to right) with probe along [0 $\overline{1}$ 0] (top) and [$\overline{1}$ 00] (bottom) after poling at -4V, with slow raster axis along [1 $\overline{1}$ 0].

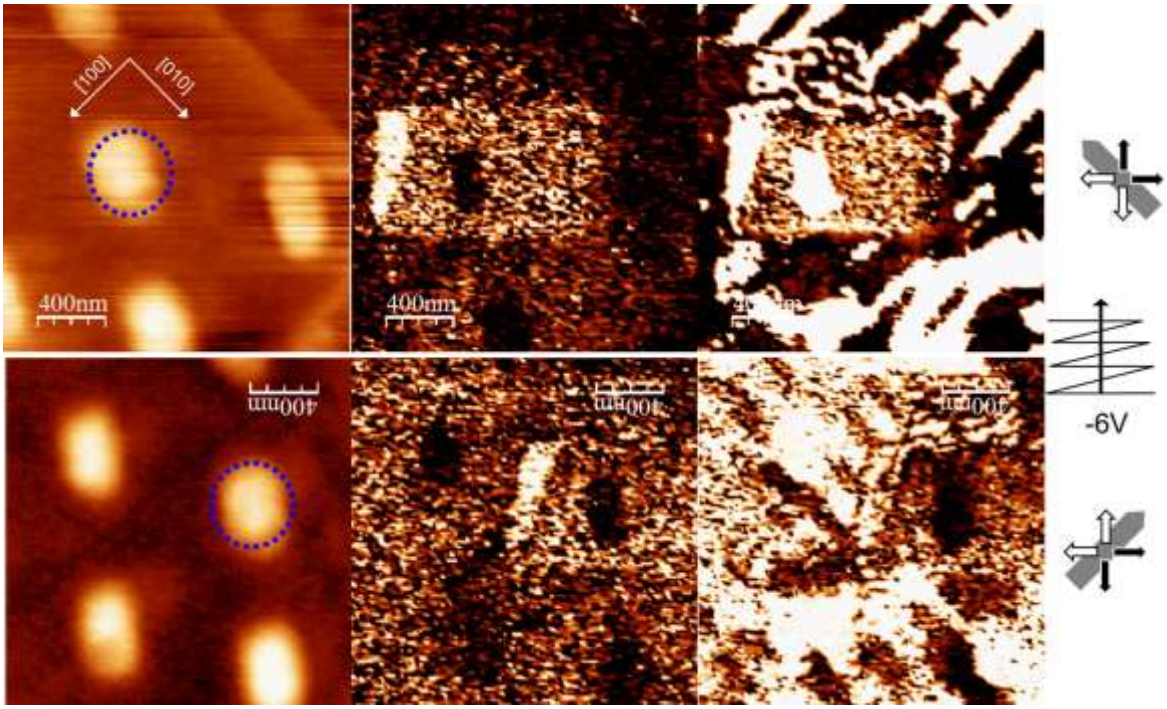

Figure S6. Topography, Vertical PFM phase, Lateral PFM phase (left to right) with probe along [0 $\bar{1}$ 0] (top) and [$\bar{1}$ 00] (bottom) after poling at -6V, with slow raster axis along [$\bar{1}$ $\bar{1}$ 0].

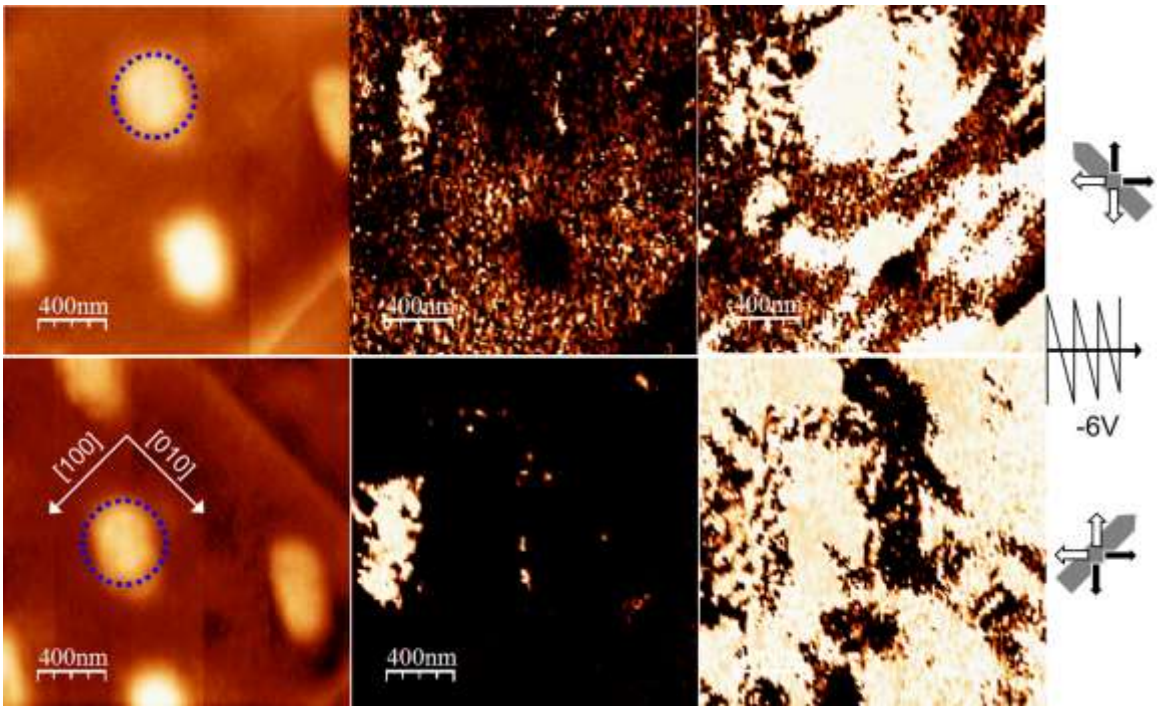

Figure S7. Topography, Vertical PFM phase, Lateral PFM phase (left to right) with probe along [0 $\bar{1}$ 0] (top) and [$\bar{1}$ 00] (bottom) after poling at -6V, with slow raster axis along [$\bar{1}$ 10].

Domain population after deterministic switching.

In order to evaluate the proportion of island switched to the desired polarization variant, domain population analysis has been performed. Determination of the island area has a critical impact on the resulting domain population. In fact, as can be seen in Figures S8a and S8b, the islands are associated with sidewalls of moderate slope: the island diameter increases from 250nm at the top surface to 600nm at the base. While during fabrication the top surface is always protected by the sacrificial layer, sidewalls experience a certain degree of exposure to the ion beam. Hence the ferroelectric properties of the sidewall will be slightly degraded. Therefore, it is reasonable to presume that deviations from the expected monodomain configuration would occur mostly in the sidewall area. In fact, by progressively increasing the threshold height used to define the nanoisland (10.5nm in S8c, 13nm in S8d, and 15.5nm in S8e), therefore progressively excluding more and more sidewall area from the analysis, the portion switched to the desired variant increases, confirming that deviations from deterministic switching occur almost exclusively in the sidewall area.

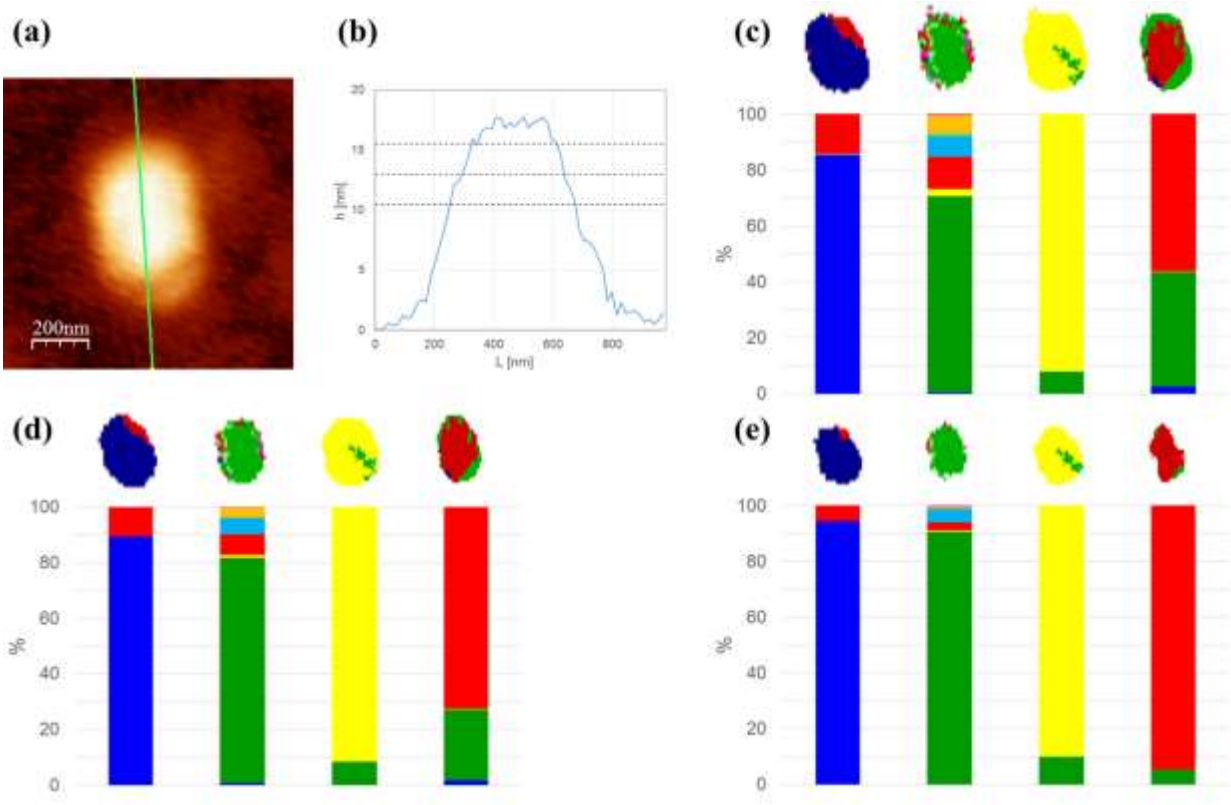

Figure S8. Topographic image of the island under investigation (a), line profile across the island (b), and stacked columns charts of the domain population after each switching experiment with threshold height set at 10.5nm (c), 13nm (d), and 15.5nm (e). The image over each stacked column is the vector PFM image of the island after each switching experiment, resulting by applying a topographic mask with height threshold as specified above.

Retention measurement.

The domain configuration achieved by deterministic switching is extremely stable. Figure S8 displays PFM imaging performed 144 days after last switching (as by Figure S5). The domain configuration is largely unchanged, indicating good retention.

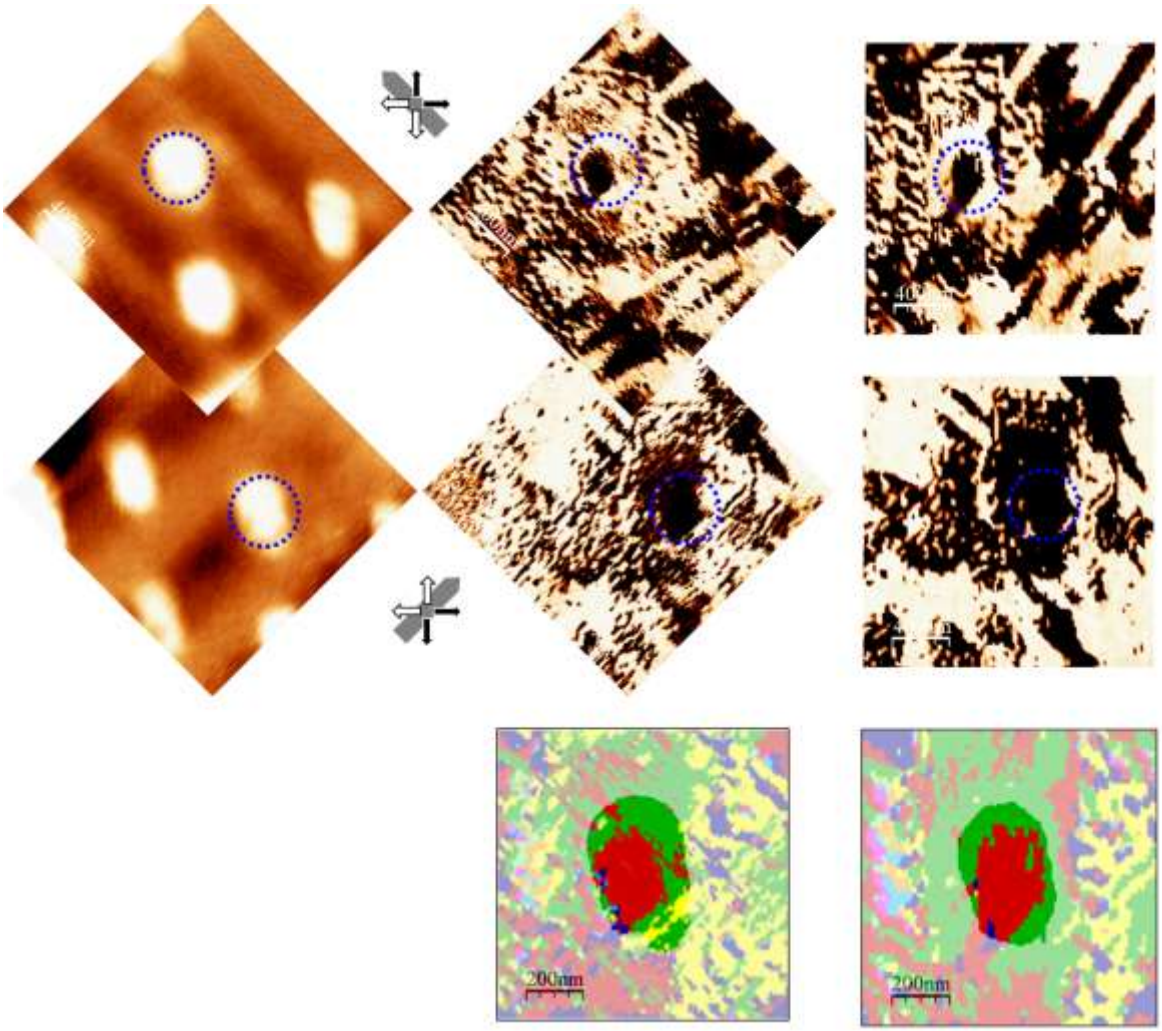

Figure S9. Topography, Lateral PFM phase after 144 days, Lateral PFM phase within the same day after switching (left to right) with probe along [0 $\bar{1}$ 0] (top) and [$\bar{1}$ 00] (center), and corresponding vector PFM images (bottom). The images on the right are exactly the same as displayed in S5, repeated here in order to make the comparison easier. The differences in domain configuration are exacerbated due to drift during image acquisition.

Deterministic switching on a second island.

Deterministic control of polarization variant is achievable in different islands, with similar degree of success. Here we present partial data of the experiment performed on a different island.

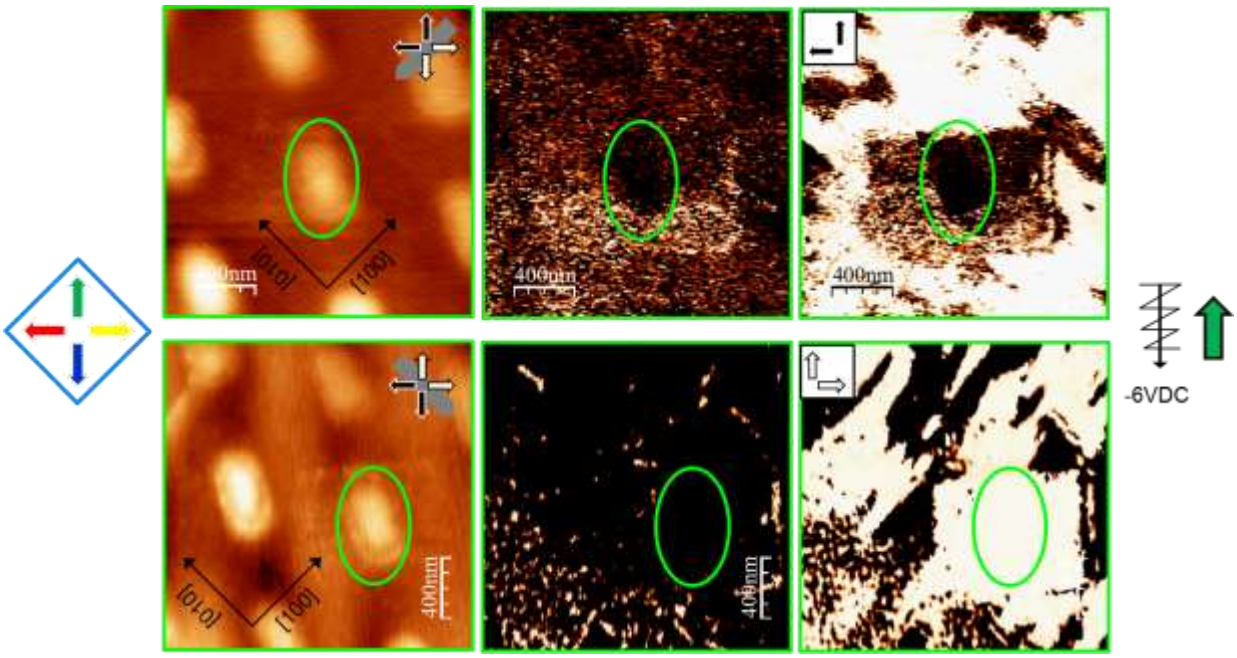

Figure S10. Topography, Vertical PFM phase, Lateral PFM phase (left to right) with probe along [$\bar{1}$ 00] (top) and [0 $\bar{1}$ 0] (bottom) after poling at -6V, with slow raster axis along [$\bar{1}$ $\bar{1}$ 0]. Expected polarization direction is [11 $\bar{1}$] (represented by arrow at the far right), matching the information from LPFM phase (insets in relative images).

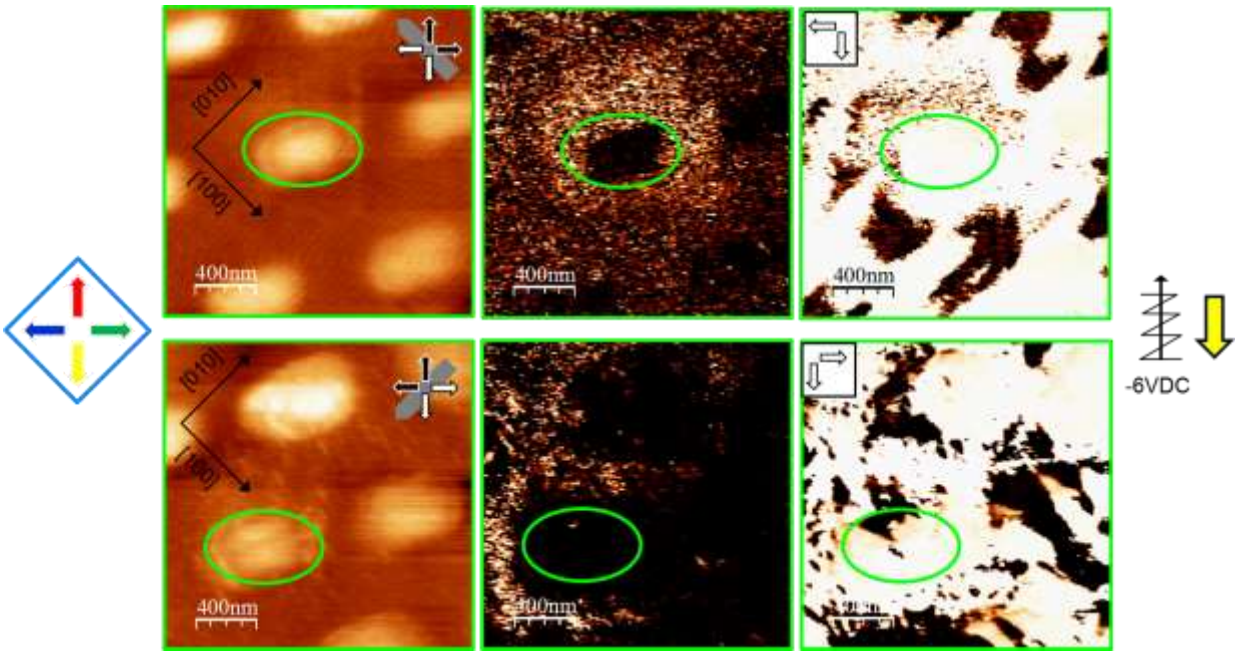

Figure S11. Topography, Vertical PFM phase, Lateral PFM phase (left to right) with probe along [$\bar{1}$00] (top) and [0$\bar{1}$0] (bottom) after poling at -6V, with slow raster axis along [$\bar{1}$10]. Expected polarization direction is [1 $\bar{1}$ $\bar{1}$] (represented by arrow at the far right), matching the information from LPFM phase (insets in relative images).

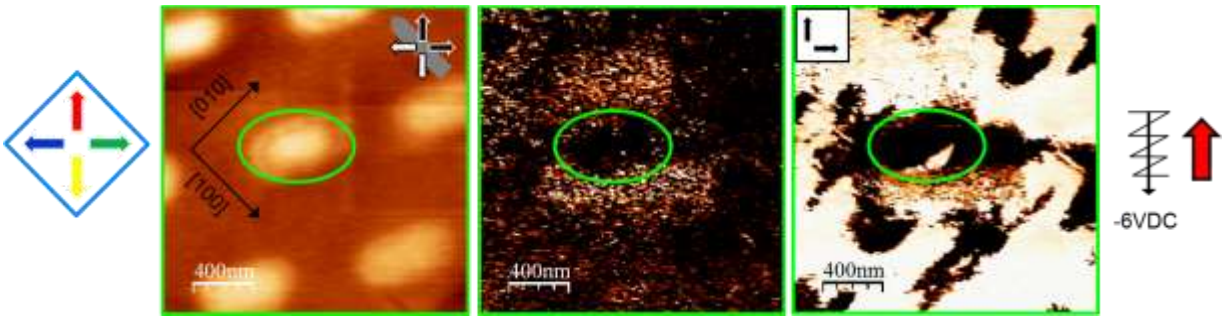

Figure S12. In-plane polarization color coding, topography, Vertical PFM phase, Lateral PFM phase (left to right) with probe along [$\bar{1}$00] after poling at -6V, with slow raster axis along [1 $\bar{1}$ 0]. Expected polarization direction is [$\bar{1}$ 1 $\bar{1}$] (represented by arrow at the far right), in agreement with the information from LPFM phase (inset in the relative image).

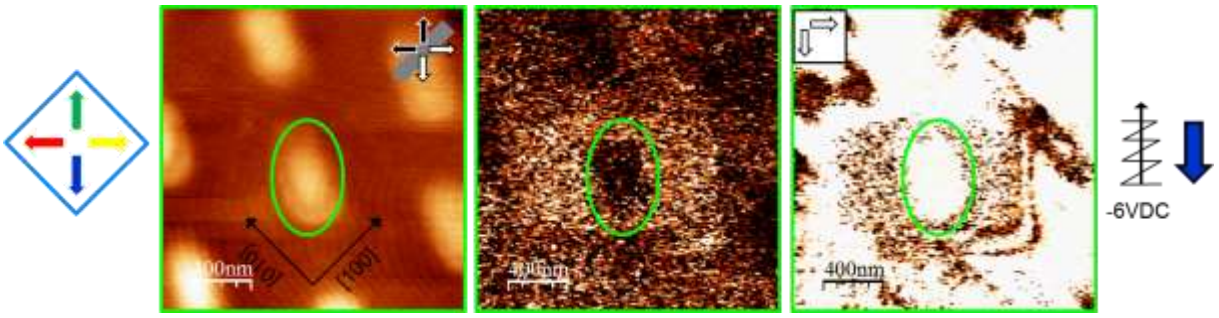

Figure S13. In-plane polarization color coding, topography, Vertical PFM phase, Lateral PFM phase (left to right) with probe along [$\bar{1}$00] after poling at -6V, with slow raster axis along [110]. Expected polarization direction is [$\bar{1}\ \bar{1}\ \bar{1}$] (represented by arrow at the far right), in agreement with the information from LPFM phase (inset in the relative image).